Peculiarities of *IV*-characteristics and magnetization dynamics in the φ_0 Josephson junction

Yu. M. Shukrinov[1,2,3], I. R. Rahmonov[1,4], and A. E. Botha[3]

[1]BLTP, Joint Institute for Nuclear Research, Dubna, Moscow Region 141980, Russia

[2]Dubna State University, Dubna 141980, Russia

[3]Department of Physics, University of South Africa, Florida, Johannesburg 1710, South Africa

[4]Umarov Physical Technical Institute, TAS, Dushanbe 734063, Tajikistan
E-mail: shukrinv@theor.jinr.ru

The φ_0 junction demonstrates a rich variety of dynamical states determined by parameters of the Josephson junction and the intermediate ferromagnetic layer. Here we find several peculiarities in the maximal amplitude of magnetic moment $\hat{m}_y$, taken at each value of the bias current, which we correlate to the features of the *IV*-characteristics of the φ_0 junction. We show that a kink behavior in the bias current (voltage) dependence of $\hat{m}_y$ along the *IV*-characteristics is related to the changes in the dynamical behavior of the magnetization precession in the ferromagnetic layer. We also demonstrate a transformation of the magnetization specific trajectories along the *IV*-curve, magnetization composite structures, and hysteretic behavior in the bias current dependence of $\hat{m}_y$. Due to the correlations between features of $\hat{m}_y$ and the *IV*-characteristics, the presented results open a way for the experimental testing of the peculiar magnetization dynamics which characterize the φ_0 junction.

Keywords: Josephson SFS junction, *IV*-characteristics, current-phase relation.

1. Introduction

The φ_0 Josephson junction [1] with the current-phase relation $I_s = I_c \sin(\varphi - \varphi_0)$ is becoming an interesting and important topic in condensed matter physics [2, 3]. The superconductor–ferromagnet–superconductor (SFS) φ_0 junctions where the phase shift φ_0 is proportional to the magnetic moment perpendicular to the gradient of the asymmetric spin-orbit potential, demonstrate a number of unique features important for superconducting spintronics and modern informational technologies [2, 4–8]. This coupling between phase and magnetic moment of the ferromagnetic layer allows one to manipulate the internal magnetic moment using the Josephson current [1, 9]. The magnetic moment also might pumps current through the φ_0 phase shift. It leads to the appearance of the dc component of superconducting current in φ_0 Josephson junction [7, 9, 10].

The application of dc voltage to the φ_0 junction produces current oscillations and consequently magnetic precession. As shown in Ref. 9, this precession may be monitored by the appearance of higher harmonics in the current–phase–relation (CPR) as well as by the presence of a dc component of the superconducting current that increases substantially near the ferromagnetic resonance (FMR). The authors stressed that

the magnetic dynamics of the SFS φ_0 junction may be quite complicated and strongly anharmonic. In contrast to these results, very simple characteristic trajectories magnetization precession in the $m_y - m_x$, $m_z - m_x$, and $m_z - m_y$ planes were recently discovered in Ref. 10. To distinguish specific shapes, some were named as "apple", "sickle", "mushroom", "fish", "moon", etc.

Recent experiments [11–13] have measures an anomalous Josephson effect, validating the φ_0 junction model and pointing to its potential uses in a variety of technologies that rely on superconducting spintronics [2, 14]. The specific nature of the coupling that occurs in the φ_0 junction allows one to manipulate the internal magnetic moment via the Josephson current, and conversely [1, 9, 15].

Previous simulations of the φ_0 junction demonstrated how the application of an external electromagnetic field could be used to tune the character of the magnetic moment precession over current intervals corresponding to specific Shapiro steps [10]. We also demonstrated the appearance of a dc component in the superconducting current and clarified how it influences the *IV*-characteristics within the resonance region, i. e., the region where the precession frequency is close to that of the Josephson frequency. The effects of Gilbert damping and spin-orbit coupling on *IV*-characteristics and magnetization precession were also studied. We also

studied factors that could affect the magnetization reversal by the superconducting current in the φ_0 junction [6, 8]. The physics of φ_0 junction was found to have many features in common with the famous Kapitza pendulum problem [7]. Most recently we were able to provide analytical criteria for magnetization reversal from predicting the conditions under which the reversal can occur [16]. In the Introduction of Ref. 16, we have given a detailed review of recent experimental and theoretical developments relating to the φ_0 junction, and we also discuss the choice of materials available for its practical realization.

This present work is an extension of some preliminary results [17]. Here we provide a more detailed investigation of the complicated dynamics that results from the unique interaction between the superconducting current and magnetic moment in the φ_0 junction. Interspersed with chaotic dynamics we find several windows of regular dynamics. In certain ranges of bias current, there are stable states of the magnetization precession, which we were able to characterize by the very specific shapes they make through projections of the phase trajectories. We also simulate how the maximal amplitude of $\hat{m}_y$ changes as the bias current is swept along the *IV*-characteristic.

We find a kink behavior in the bias current (voltage) dependence of the maximal $\hat{m}_y$ which origin is related to the change of the dynamical behavior of the magnetization in ferromagnetic layer. The characteristic trajectories in the $m_y - m_x$, $m_z - m_x$, and $m_z - m_y$ planes were recently discussed in Ref. 10. However, the kinks that occur in $\hat{m}_y$, and specifically their origin, have not been discussed before. As was alluded to in Ref. 10, these characteristic trajectories offer a unique possibility to control the magnetization dynamics via an external bias current. Here we show that similar shaped kinks have a common origin due to the underlying dynamics. We also demonstrate how specifically shaped trajectories transform from one shape into another, the manifestation of composite structures, and hysteretic behavior.

2. Model and methods

In the considered SFS structure the superconducting phase difference φ and magnetization **M** of the ferromagnetic (F) layer are coupled dynamical variables. The system of equations describing their dynamics is obtained from the Landau–Lifshitz–Gilbert (LLG) equation, the expression for the bias current of the resistively and capacitively shunted junction (RCSJ) model, and the Josephson relation between the phase difference and voltage.

Magnetization dynamics is described by the LLG equation [18]

$$\frac{d\mathbf{M}}{dt} = -\gamma \mathbf{M} \times \mathbf{H}_{\text{eff}} + \frac{\alpha}{M_0}\left(\mathbf{M} \times \frac{d\mathbf{M}}{dt}\right), \quad (1)$$

where γ is the gyromagnetic ratio, α is Gilbert damping parameter, $M_0 = |\mathbf{M}|$, and $\mathbf{H}_{\text{eff}}$ is the effective magnetic field. Here we have used the model developed in Refs. 9, 15,

where it is assumed that the gradient of the spin-orbit potential is along the easy axis of magnetization, which is taken to be along $\hat{z}$. In this case effective magnetic field is determined by

$$H_{\text{eff}} = \frac{K}{M_0}\left[Gr\sin\left(\varphi - r\frac{M_y}{M_0}\right)\hat{y} + \frac{M_z}{M_0}\hat{z}\right], \quad (2)$$

where K is the anisotropic constant, $G = E_J / (KV)$, V is the volume of F layer, $E_J = \Phi_0 I_c / (2\pi)$ is the Josephson energy, Φ_0 is the flux quantum, I_c is the critical current, $r = l v_{so} / v_F$ is parameter of spin-orbit coupling, $l = 4hL / \hbar v_F$, L is the length of F layer, h is the exchange field of the F layer, the parameter v_{so} / v_F characterizes a relative strength of spin-orbit interaction. We note that the second term inside of the sine function, i.e., rM_y / M_0 is the above mentioned phase shift φ_0.

In order to describe the full dynamics of SFS structure the LLG equations should be supplemented by the equation for phase difference φ, i.e., equation of RCSJ model for bias current and Josephson relation for voltage. According to the extended RCSJ model [15], which takes into account time derivative of phase shift φ_0, the current flowing through the system in underdamped case is determined by

$$I = \frac{\hbar C}{2e}\frac{d^2\varphi}{dt^2} + \frac{\hbar}{2eR}\left[\frac{d\varphi}{dt} - \frac{r}{M_0}\frac{dM_y}{dt}\right] + I_c\sin\left(\varphi - \frac{r}{M_0}M_y\right),$$

$$(3)$$

where I is the bias current, C and R are the capacitance and the resistance of the Josephson junction, respectively.

The Josephson relation for voltage is given by

$$\frac{\hbar}{2e}\frac{d\varphi}{dt} = V. \quad (4)$$

Using (1)–(4), we can write the system of equations in normalized variables, which describes the dynamics of φ_0 junction as

$$\dot{m}_x = \frac{\omega_F}{1+\alpha^2}\left\{-m_y m_z + Grm_z\sin(\varphi - rm_y) - \right.$$
$$\left. -\alpha\left[m_x m_z^2 + Grm_x m_y\sin(\varphi - rm_y)\right]\right\},$$

$$\dot{m}_y = \frac{\omega_F}{1+\alpha^2}\left\{m_x m_z - \alpha\left[m_y m_z^2 - Gr(m_z^2 + m_x^2)\sin(\varphi - rm_y)\right]\right\},$$

$$\dot{m}_z = \frac{\omega_F}{1+\alpha^2}\left\{-Grm_x\sin(\varphi - rm_y) - \right.$$
$$\left. -\alpha\left[Grm_y m_z\sin(\varphi - rm_y) - m_z(m_x^2 + m_y^2)\right]\right\},$$

$$\dot{V} = \frac{1}{\beta_c}\left[I - V + r\dot{m}_y - \sin(\varphi - rm_y)\right],$$

$$\dot{\varphi} = V,$$

$$(5)$$

where $m_{x,y,z} = M_{x,y,z} / M_0$ and satisfy the constraint $\sum_{i=x,y,z} m_i^2(t) = 1$, $\beta_c = 2eI_cCR^2$ is the McCumber parameter. In order to use the same time scale in the LLG and RCSJ equations, we have normalized time to the ω_c^{-1}, where $\omega_c = 2eI_cR / \hbar$, and $\omega_F = \Omega_F / \omega_c$ is the normalized frequency of ferromagnetic resonance ($\Omega_F = \gamma K / M_0$). Bias current is normalized to the critical current I_c and voltage V — to the $V_c = I_cR$. The system of equations (5) is solved numerically using the fourth-order Runge–Kutta method at fixed value of current $I = 0$ in time interval $[0,1500]$ with the timestep $\delta t = 0.005$. We use the initial conditions $m_x = 0$, $m_y = 0$ $m_z = 1$, $V = 0$, $\varphi = 0$, and as the results, we obtain $m_i(t)$, $V(t)$, and $\varphi(t)$ as the functions of time. Then the value of bias current is increased for the current step the $\delta I = 0.00005$ and procedure is repeating. The obtained values of m_x, m_y m_z, V and φ at time $t = 1500$ for the current I, are used as the initial conditions for the value of $I + \delta I$. During the calculation we have increased a bias current until I_{max} and then decreased to zero. In order to calculate the IV-characteristic, we average the voltage in time interval $[200,1500]$ at each value of I. To investigate the resonance behavior of the system we calculate the maximal amplitude of magnetic moment in time domain $\hat{m}_y$ at each value of the bias current I and plot it as a function $\hat{m}_y(I)$.

3. Kinks in the *IV*-characteristics and their origin

Due to interaction between the superconducting current and the magnetization in the ferromagnetic layer, the φ_0 Josephson junction exhibits a rich, complicated dynamics, which can be strongly anharmonic and even chaotic [9, 10, 15]. On the other hand, as has been demonstrated in Ref. 20, the precession of the magnetic moment in some current intervals along IV-characteristics may be relatively simple and harmonic [10]. Here we concentrate on the interaction between the Josephson current and ferromagnetic layer magnetization and on some of the peculiarities of the magnetization dynamics which may be manifested in the experimentally measured IV-characteristics of such systems. The magnetization dynamics is characterized by its maximal amplitude $\hat{m}_y$ taken at each value of the bias current along the IV-characteristics.

In Fig. 1 we present a part of IV-characteristics together with the maximal amplitude $\hat{m}_y$ with decrease in bias current at $I > I_c$. All calculations in this paper were done at the following parameters of the system: $G = 1$, $r = 1$, $\beta_c = 25$, $\alpha = 0.01$. Along with chaotic parts (see, particularly, the left side of the figure), reflecting complex magnetization precessions, we see a regular variation of $\hat{m}_y$ with the bias current. We note, that the positions of the peculiarities in the IV-characteristics coincide with the positions of the specific behavior of maximal amplitude of $\hat{m}_y$ as a function
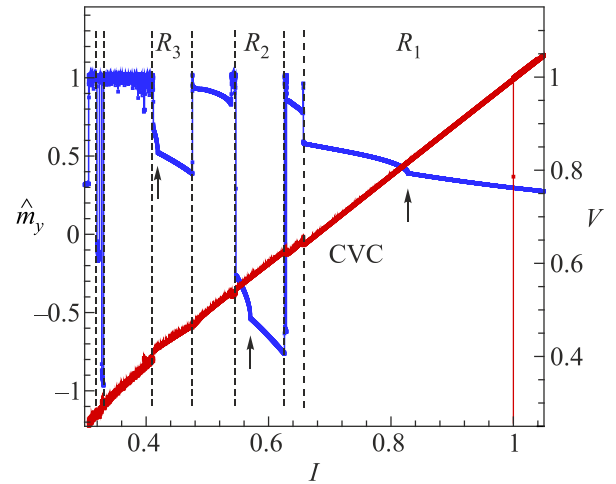

Fig. 1. Part of the *IV*-characteristic of the φ_0 junction in the ferromagnetic resonance region ($\omega_F = 0.5$) together with the maximal amplitude $\hat{m}_y$ with decrease in bias current along the *IV*-curve. Arrows show the kinks in the $\hat{m}_y(I)$ dependence.

of bias current. An interesting feature of this $\hat{m}_y(I)$ dependence are the kinks shown by the arrows.

To stress these kink peculiarities, we show in Fig. 2 the V-dependence of the maximal amplitude $\hat{m}_y$ along the IV-characteristics of the φ_0 junction at three different values of the ferromagnetic resonance frequency: $\omega_F = 0.4$, 0.5, and 0.6. In all cases we can see very clear the kinks on either
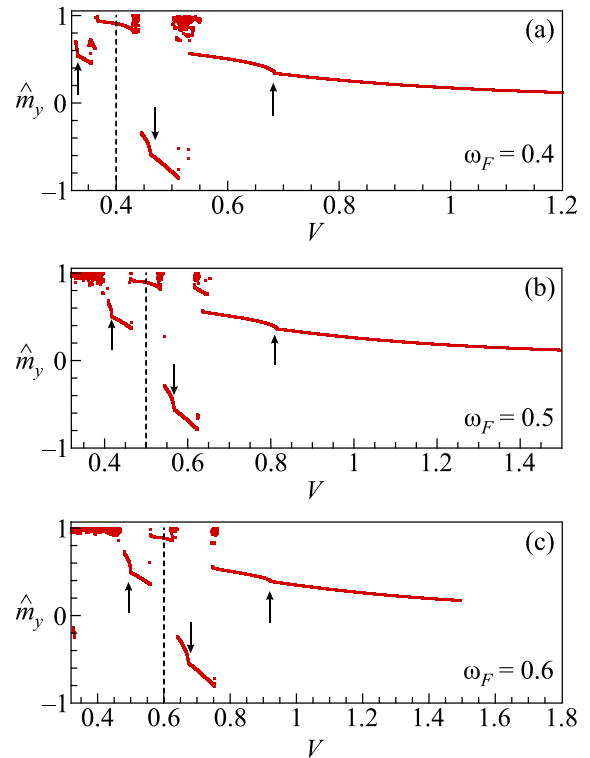

Fig. 2. *V*-dependence of the maximal amplitude $\hat{m}_y$ with a decrease of the bias current along the *IV*-characteristics of the φ_0 junction in the ferromagnetic resonance region at different values of the resonance frequency, indicated by dashed lines.
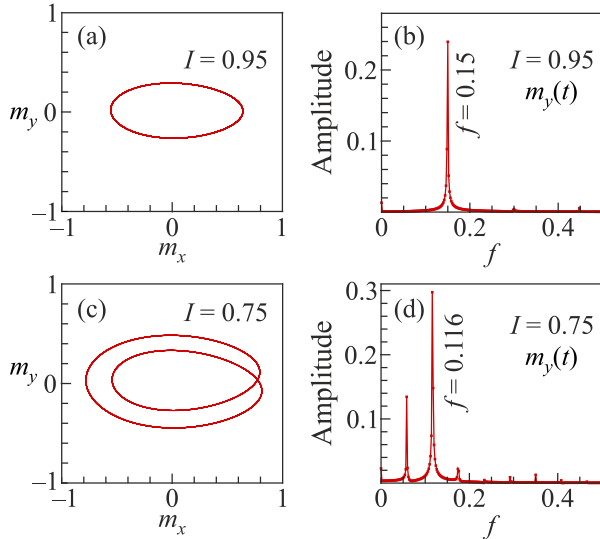
Fig. 3. Magnetization trajectories in $m_y - m_x$ plane for regular region R_1 and results of FFT analysis of the temporal dependence of m_y. The value of current at the corresponded points is indicated in the figures.

Fig. 4. Magnetization trajectories in $m_z - m_x$ plane for regular region R_2 and results of FFT analysis of the temporal dependence of m_y: (a), (b) at $I = 0.6$; (c), (d) at $I = 0.555$.

side of the resonance frequency ω_F in the R_2 and R_3 regions. Such a shift in the kink position indicates their relation to the ferromagnetic resonance. A kink in the region R_1 is also manifested, but it has no symmetric counterpart due to the transition of the Josephson junction to the zero voltage state. One of the the main purposes of the present paper is to explain the origin of the kink.

In Fig. 3 we demonstrate the magnetization trajectories in the $m_y - m_x$ plane and the corresponding results of FFT analysis of the temporal dependence of m_y in the regular region R_1, at $I = 0.95$ (a), (b) and $I = 0.75$ (c), (d), i.e., to the right and left sides of the kink, respectively. We find that the kink is the bifurcation point between the two types of trajectories, i.e., as the system goes from period one to period two behavior.

In Figs. 3(b), (d) we present results of FFT analysis of the time dependence of the magnetization component m_y at different bias currents corresponding to the dynamics before and after the kink. At $I = 0.75$ an additional frequency $f = f_J / 2$ appears in comparison to the case at $I = 0.95$, confirming the period doubling.

Different types of magnetization trajectories in the $m_y - m_x$, $m_z - m_x$, and $m_z - m_y$ planes, realized along the *IV*-characteristics were found in Ref. 10, such as "apple", "sickle", "mushroom", "fish", and "moon", called like that for distinctness. But the kinks in $\hat{m}_y$ and their origin were not discussed at that time. It was mentioned there that the specific trajectories demonstrate a unique possibility of controlling the magnetization dynamics via external bias current. Here we show the similarity in the appearance of the different kinks and stress that their origin is related to the transformation in the magnetization dynamics. In Fig. 4 we demonstrate the magnetization trajectories around the kink in the R_2 region, which present the "apple" type at
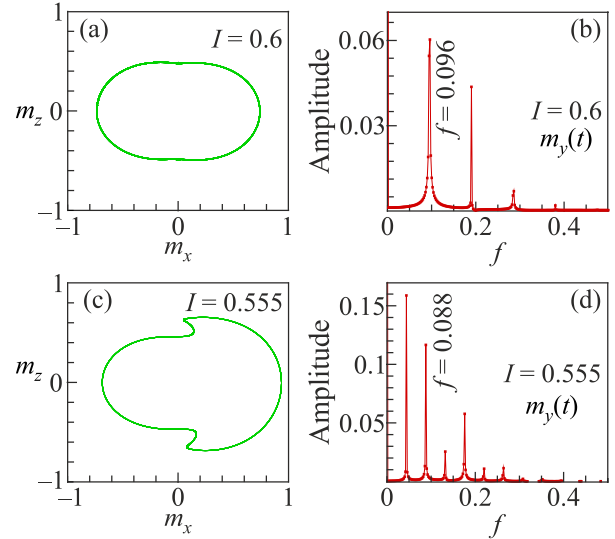
$I = 0.6$ before the kink and the "mushroom" type after kink at $I = 0.555$. The results of FFT analysis [see Figs. 4(b), (d)] show the doubling of the period of trajectories in case of the "mushroom".

Actually, such a transformation of the "apple"-type trajectory to the "mushroom" type happens over a large bias current interval, and we will discuss this in the next section. In Fig. 5 we first show time dependence of the m_y very close
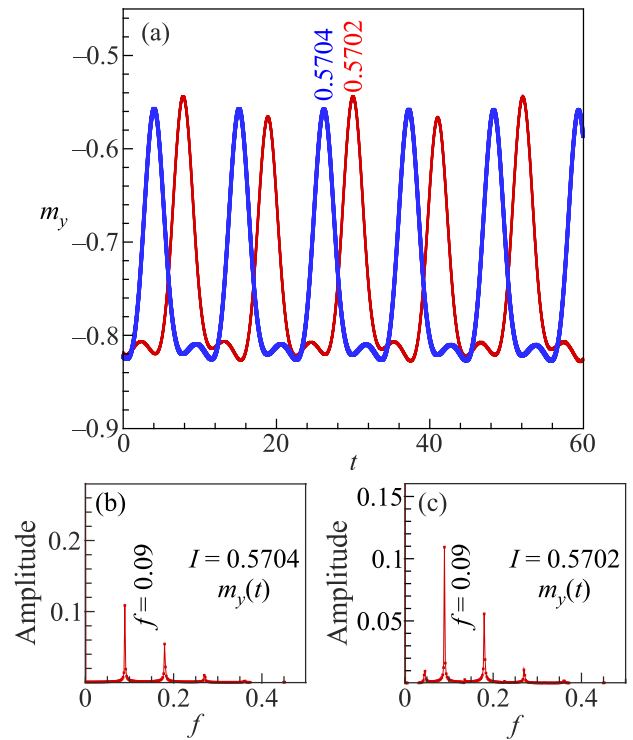

Fig. 5. (a) Time dependence of the m_y at $I = 0.5704$ and $I = 0.5702$; (b) FFT analysis of time dependence of m_y at $I = 0.5704$; (c) The same as (b) at $I = 0.5702$.
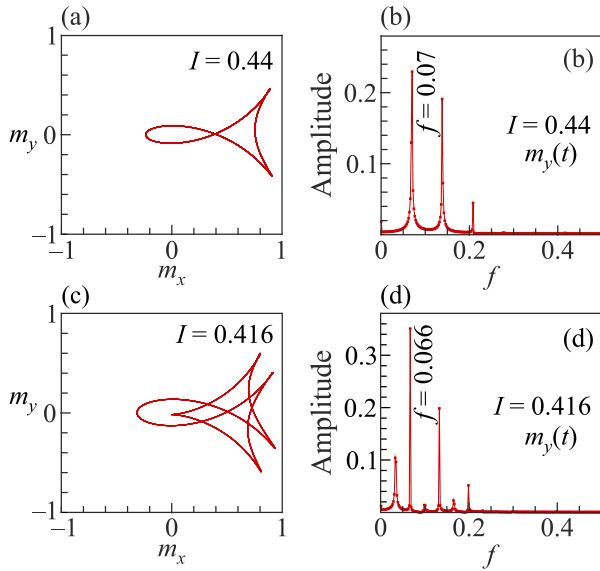
Fig. 6. Magnetization trajectories in $m_y - m_x$ plane for regular region R_3 and results of FFT analysis of temporal dependence of m_y. The value of current at the corresponded points is indicated in the figures.

Fig. 7. Transformation of the "apple"-type trajectory to the "mushroom" one near kink at $I = 0.5703$. (a) "Apple"-type trajectory before kink; (b) Enlarged part of (a), demonstrating scroll; (c) Trajectory transformation after kink; (d) Enlarged part of (c) near scroll.

to the kink, just at current step before ($I = 0.5704$) and after ($I = 0.5702$) the kink. We see that the difference is related to the modulation of the time dependence after the kink. FFT analysis [Figs. 5(b), (c)] again confirms this transformation in the dynamics of the system through the appearance of the corresponding small peaks.

In Fig. 6 we demonstrate that the kink in the region R_3 is related to the transformation of the "fish"-type trajectory, realized at $I = 0.44$, to the "double fish" trajectory, at $I = 0.416$. Results of FFT analysis presented in Figs. 6(b), (d) show the doubling of the magnetization precession period in the case of "double fish"-type trajectory.

The presented results thus demonstrate that the kinks in $\hat{m}_y$, in all three of the considered regular regions R_1, R_2 and R_3, are related to period doubling bifurcations of the specific precession trajectories.

4. Transformation of the magnetization trajectories and composite dynamics

The application of dc voltage to the φ_0 junction produces current oscillations and consequently magnetic precession. As shown in Refs. 9, 15, this precession may be monitored by the appearance of higher harmonics in the current-phase relation as well as by the presence of a dc component in the superconducting current. The latter increases substantially near the ferromagnetic resonance (FMR). In contrast to Konschelle and Buzdin [9, 15], who stressed that the magnetic dynamics of the SFS φ_0 junction may be quite complicated and strongly anharmonic, in Ref. 10 we demonstrated that the precession of the magnetic moment in certain current intervals along *IV*-characteristics may be very simple and harmonic.
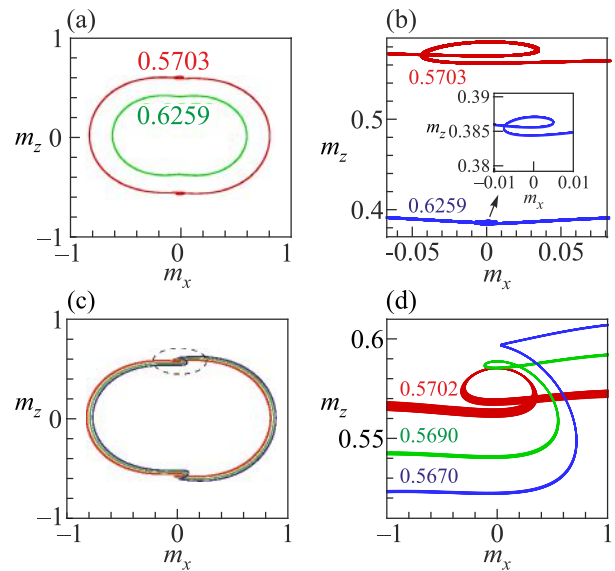
In this section we discuss two peculiarities of the magnetization dynamics. The first peculiarity is related to the transformations that occur between the two types of the trajectories. We found that such transformations happen continuously. As we have seen above, the region R_2 within bias current interval [0.54675,0.6259] demonstrates a kink behavior at $I = 0.5703$. Going down along *IV*-characteristic, we observe first the "apple"-type trajectory, and then after the kink a "mushroom" type, i.e., in the $m_z - m_x$ plane. In Fig. 7(a) we show the trajectory of the magnetization at the boundaries of the interval [0.5703,0.6259] and see that the amplitude of m_z and m_x is increased with a decrease in I.

At the point where the magnetization pass the point with the $m_x = 0$, we can see a scroll structure. On the boundary of the above mentioned two intervals, the scroll structure at $I = 0.5703$ is widening. It is demonstrated in Fig. 7(b), where a zoomed part of the trajectories for two boundary values of bias current is presented. In both cases we see a scroll, which reminded letter "e". After the kink is passed, the scroll is transformed and reminds one of a reflected letter "e" now. In the current interval [0.54675,0.5703] the "apple"-type trajectory continuously transforms to the "mushroom" one. This transformation is demonstrated in Fig. 7(c), where the trajectories for three values of current are presented. In Fig. 7(d) the zoomed part of trajectories closed to the point $m_x = 0$ is shown [this region is marked with the dashed ellipse in Fig. 7(c)]. As we can see, the scroll structure disappears continuously throughout the transformation.

The second peculiarity is related to the creation of the composite type of the trajectory. An example of such magnetization dynamics appears in the current interval
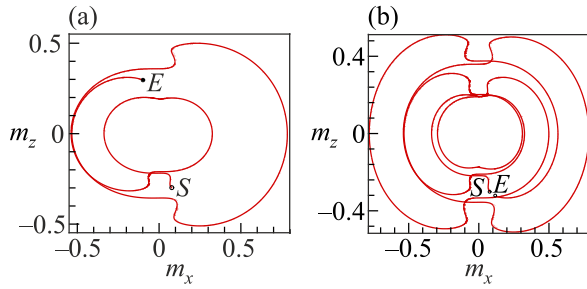
Fig. 8. Realization of composite type trajectory at $I = 0.6268$: (a) during the first 10000 time units; (b) during the second 20000 time units. Points S and E mean starting and ending points of recording.

[0.6268,0.6288] between regions R_2 and R_3 and is demonstrated in Fig. 8. We see a realization of composite-type trajectory, i.e., different type of precessions are realizing in during one period: "apple", large, small "left and right mushrooms". Starting from the point S, in during the first 10000 time units the magnetization describes first an "apple", then large "right mushroom" [see Fig. 8(a)], then it continues a precession along small "left mushroom", small "right mushrooms" and large "left mushrooms" [see Fig. 8(b)]. We stop recording of the time dependence close to the end of the period after 20000 time units (see point E). We note that the composite structures of different type trajectories may appear in different parts of *IV*-characteristics by changing the system's parameters.

5. Hysteresis in $\hat{m}_y(I)$ dependence

Another peculiarity we found in the current dependence of the maximal magnetization of the φ_0 junction is an appearance a sequence of hysteresis at different ferromagnetic resonance frequencies. In Fig. 9 we show the bias current dependence of $\hat{m}_y$ for three frequencies: (a) $\omega_F = 0.5$, (b) $\omega_F = 1$ and (c) $\omega_F = 1.5$. They demonstrate that the difference in the bias current dependence of $\hat{m}_y$ for increase and decrease the bias current is appeared. We see that at $\omega_F = 0.5$ the McCumber type of hysteresis known for *IV*-characteristics of underdamped Josephson junctions is manifested only, while with increase in frequency an additional hysteresises start manifest themselves [see Fig. 9(b)]. At $\omega_F = 1.5$ we observe a rather large and very pronounced hysteresis at $I > I_c$. There are two more small hysteresises which we do not mark in Figs. 9(b), (c).

An important point is that this peculiarity in the bias current dependence of $\hat{m}_y$ manifests itself in the corresponded *IV*-characteristics also. Below we stress such a manifestation in the the *IV*-curve, particularly, we show in Fig. 10 the enlarged part of *IV*-characteristics which demonstrate the manifestation of the starting and ending points of hysteresis, indicated in Fig. 9(c). We show there the stating point [S_1, see Fig. 10(a)] of the largest hysteresis at $\omega_F = 1.5$, which is ending with a chaotic behavior at point E_1 [Fig. 10(b)].
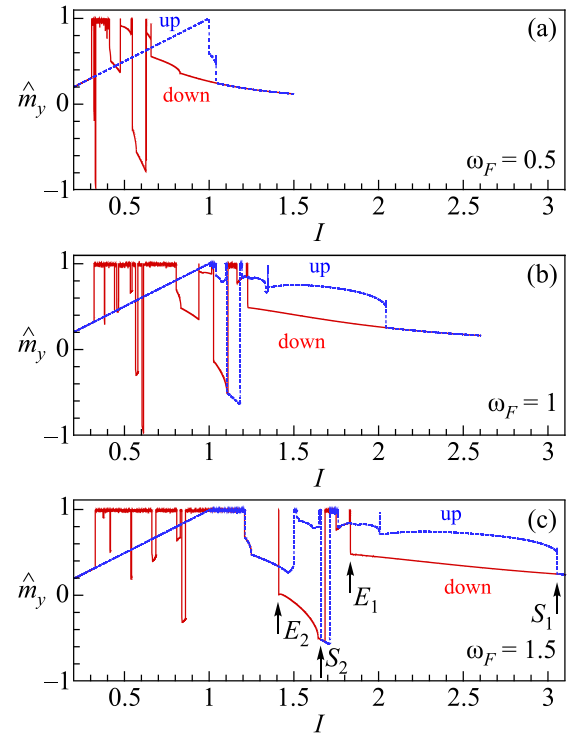

Fig. 9. Bias current dependence of $\hat{m}_y$ in the increase (dotted) and the decrease (solid) bias current for: (a) $\omega_F = 0.5$, (b) $\omega_F = 1$, (c) $\omega_F = 1.5$.

We also demonstrate the manifestation of the ending point E_2 of another big hysteresis at $\omega_F = 1.5$ in Fig. 10(c).

The *IV*-characteristics are measured experimentally, so the results presented above open a way for experimental testing of the peculiarities pronounced in the magnetization
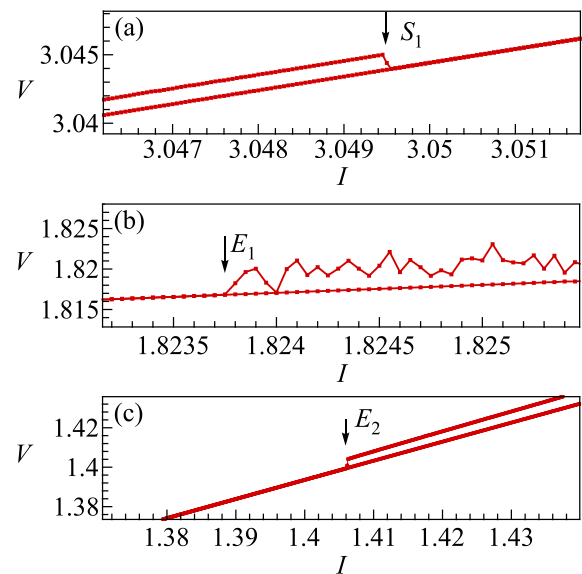

Fig. 10. Manifestation of the hysteretic behavior in the *IV*-characteristic near points, marked in Fig. 9(c). (a) Starting point of the first hysteresis; (b) Ending point of the first hysteresis; (c) Ending point of the second large hysteresis.

dynamics of φ_0 Josephson junctions. The question concerning the details of the hysteresis appearance and its dependence on the parameters of the system will be addressed elsewhere.

6. Conclusions

We have studied the interaction between the superconducting current and magnetic moment in a φ_0 junction and investigated the maximal amplitude of the magnetization momement $\hat{m}_y(I)$, where I is the bias current. We found a kink behavior in the bias current (voltage) dependence of $\hat{m}_y(I)$ along the *IV*-characteristics. Analysis of the magnetization precession dynamics and trajectories revealed that the origin of the kinks can be related to changes in the dynamical behavior of the magnetization precession in ferromagnetic layer. Found effects concerning the transformation of the magnetization specific trajectories along the *IV*-curve, magnetization composite structures, and hysteretic behavior in the bias current dependence of $\hat{m}_y$ open several interesting directions for future investigations. Due to the correlations between the discovered features of $\hat{m}_y$ and the *IV*-characteristics, the presented results open a way for the experimental testing of the peculiar magnetization dynamics which characterize the φ_0 junction.

We note that in our model the interaction between the Josephson current and the magnetization is determined by the parameter $G = E_J / (K\mathcal{V})$, which describes the ratio between the Josephson energy and the magnetic anisotropy energy and spin-orbit interaction. The value of the Rashba-type spin-orbit interaction parameter in a permalloy doped with platinum [21] up to 10 %, in the ferromagnets without inversion symmetry, like MnSi or FeGe, usually estimated in the range $0.1-1$, the value of the Γ in the material with weak magnetic anisotropy $K \sim 4 \cdot 10^{-5}$ K$\cdot$A^{-3} [22], and a junction with a relatively high critical current density of $(3 \cdot 10^5 - 5 \cdot 10^6)$ A$\cdot$cm^{-2} [23] is in the range $1-100$. It gives the set of ferromagnetic layer parameters and junction geometry that make it possible to reach the values used in our numerical calculations, for the possible experimental observation of the predicted effect.

Acknowledgments

1. A. Buzdin, *Phys. Rev. Lett.* **101**, 107005 (2008).
2. Jacob Linder and J. W. A. Robinson, *Nat. Phys.* **11**, 307 (2015).
3. O. Durante, R. Citro, C. Sanz-Fernández, C. Guarcello, I. V. Tokatly, A. Braggio, M. Rocci, N. Ligato, V. Zannier, L. Sorba, F. S. Bergeret, F. Giazotto, E. Strambini, and A. Iorio, *Nat. Nanotechnol.* (2020).
4. A. I. Buzdin, *Rev. Mod. Phys.* **77**, 935 (2005).
5. A. A. Golubov, M. Y. Kupriyanov, and E. Ilichev, *Rev. Mod. Phys.* **76**, 411 (2004).
6. Yu. M. Shukrinov, I. R. Rahmonov, K. Sengupta, and A. Buzdin, *Appl. Phys. Lett.* **110**, 182407 (2017).
7. Yu. M. Shukrinov, A. Mazanik, I. R. Rahmonov, A. E. Botha, and A. Buzdin, *EPL* **122(3)**, 37001 (2018).
8. P. Kh. Atanasova, S. A. Panayotova, I. R. Rahmonov, Yu. M. Shukrinov, E. V. Zemlyanaya, and M. Bashashin, *JETP Lett.* **110**, 722 (2019).
9. F. Konschelle and A. Buzdin, *Phys. Rev. Lett.* **102**, 017001 (2009).
10. Yu. M. Shukrinov, I. R. Rahmonov, and K. Sengupta, *Phys. Rev. B* **99**, 224513 (2019).
11. D. Szombati, S. Nadj-Perge, D. Car, S. R. Plissard, E. P. A. M. Bakkers, and L. P. Kouwenhoven, *Nature Phys.* **12**, 568 (2016).
12. A. Assouline, C. Feuillet-Palma, N. Bergeal, T. Zhang, A. Mottaghizadeh, A. Zimmers, E. Lhuillier, M. Eddrie, P. Atkinson, M. Aprili, and H. Aubin, *Nat. Commun.* **10**, 126 (2019).
13. W. Mayer, M. C. Dartiailh, J. Yuan, K. S. Wickramasinghe, E. Rossi, and J. Shabani, *Nat. Commun.* **11**, 212 (2020).
14. Subhajit Pal and Colin Benjamin, *EPL* **126**, 57002 (2019).
15. F. Konschelle and A. Buzdin, *Phys. Rev. Lett.* **102**, 017001 (2009); F. Konschelle and A. Buzdin, *Phys. Rev. Lett.* **123**, 169901 (2019).
16. A. A. Mazanik, I. R. Rahmonov, A. E. Botha, and Yu. M. Shukrinov, *Phys. Rev. Appl.* **14**, 014003 (2020).
17. Yu. M. Shukrinov, I. R. Rahmonov, and A. E. Botha, in: *Nanophysics and Nanoelectroncs: Proceedings of the XXVI International Symposium*, Nizhniy Novgorod State University, Nizhniy Novgorod 10–13 March (2020), Vol. 1, p. 21.
18. E. M. Lifshitz and L. P. Pitaevskii, *Course of Theoretical Physics*, *Theory of the Condensed State*, Butterworth Heinemann, Oxford (1991), Vol. 9.
19. D. Rabinovich, I. Bobkova, A. Bobkov, and M. Silaev, *Phys. Rev. Lett.* **123**, 207001 (2019).
20. Yu. M. Shukrinov, Majed Nashaat, I. R. Rahmonov, and K. Kulikov, *JETP Lett.* **110**, 160 (2019).
21. A. Hrabec, F. J. T. Gonçalves, C. S. Spencer, E. Arenholz, A. T. N'Diaye, R. L. Stamps, and Christopher H. Marrows, *Phys. Rev. B* **93**, 014432 (2016).
22. A. Yu. Rusanov, M. Hesselberth, J. Aarts, and A. I. Buzdin, *Phys. Rev. Lett.* **93**, 057002 (2004).
23. J. W. A. Robinson, F. Chiodi, M. Egilmez, G. B. Halász, and M. G. Blamire, *Sci. Rep.* **2**, 699 (2012).

Особливості вольт-амперних характеристик та динаміка намагніченості джозефсонівських φ₀ контактів

Yu. M. Shukrinov, I. R. Rahmonov,
A. E. Botha

Джозефсонівські φ₀ контакти демонструють велике різноманіття динамічних станів, які визначаються параметрами джозефсонівського переходу й посереднього феромагнітного шару. Знайдено низку особливостей у поведінці максимальної амплітуди магнітного моменту $\hat{m}_y$ для кожного значення струму зміщення. Ці особливості співвіднесено з особливостями вольт-амперної характеристики φ₀ контакту. Показано, що поведінка кінку в залежності $\hat{m}_y$ від струму (напруги) вздовж *IV*-кривої пов'язана зі зміною динамічної поведінки прецесії намагніченості у феромагнітному шарі. Продемонстровано трансформацію специфічних траєкторій намагніченості вздовж *IV*-кривої, намагніченості композитних структур та гістерезисної поведінки залежності $\hat{m}_y$ від струму зміщення намагніченості. Результати, які приведено, внаслідок кореляції між особливостями $\hat{m}_y$ та *IV*-характеристиками дозволяють експериментальну перевірку специфічної динаміки намагніченості, яка характеризує φ₀ контакти.

Ключові слова: SFS джозефсонівські контакти, вольт-амперні характеристики, співвідношення струм–фаза.